Materials Research. 2022; 25:e20210414
DOI: https://doi.org/10.1590/1980-5373-MR-2021-0414

Cryogenic and Room Temperature ECAP Consolidation of Blended Elemental Powders of Aluminum and Copper

Ricardo Sanson Namur[a]*, Maxwell Silva Azevedo[a], Marcel Tadashi Izumi[a], Denilson Jose Marcolino de Aguiar[b], Kahl Dick Zilnyk[c], Osvaldo Mitsuyuki Cintho[a]

[a]Universidade Estadual de Ponta Grossa, Departamento de Engenharia de Materiais, Av. Carlos Cavalcanti, 4748, Campus Universitário de Uvaranas, CEP 84030-900, Ponta Grossa, PR, Brasil.
[b]Universidade Tecnológica Federal do Paraná, CEP 84017-220, Ponta Grossa, PR, Brasil.
[c]Instituto Tecnológico de Aeronáutica, Departamento de Materiais e Processos, Praça Marechal Eduardo Gomes, 50, Vila das Acacias, CEP 12228-900, São José dos Campos, SP, Brasil.

Received: August 12, 2021; Revised: February 4, 2022; Accepted: February 19, 2022

The effect of temperature was investigated on the consolidation of blended elemental powders of aluminum and copper by equal channel angular pressing (ECAP). Aluminum and Copper powders (1:1% vol.) were blended and consolidated in a 90° ECAP die at room (RT) and cryogenic temperatures (CT - ~77 K). ECAP samples were pressed until 4 passes at room temperature in route Bc. As a reference, a sample was obtained by conventional uniaxial pressing. The obtained results indicated a much denser (>99.5%) and harder structure by cryogenic ECAP. The hardness after one pass at CT was comparable with 4 passes at room temperature. Tensile tests performed at CT for materials with similar chemical composition showed a simultaneous increase in strength and ductility at CT, corroborating the results obtained by ECAP. The partial suppression of dynamic recovery and the activation and the transition between deformation mechanisms at CT, as well as stacking fault energies (SFE) of such metals, played an important role in these results. Copper presented a much higher capability of strain hardening than aluminum, due to its lower SFE and much lower homologous temperature. X-ray diffraction indicated a strong correlation between the variation of average microstrain and the variation of hardness on both metals. The results of this study demonstrated the great potential of the application of very low temperatures for the obtaining of deformation metal-metal composites.

Keywords: *Cryogenic deformation, equal channel angular pressing, powder consolidation, deformation processed metal-metal composite.*

1. Introduction

The obtaining of bulk materials from powders is being used for a long time. The advantage of avoiding solidification issues, such as casting defects and segregation, has motivated the development of this technique for processing metals, especially the ones with high melting temperatures. Besides the great improvements on these techniques, the residual porosities are still an issue for conventional powder metallurgy (PM).

With the objective of avoiding conventional PM problems, Severe Plastic Deformation (SPD) techniques that were previously designed for processing of bulk materials, started to be used for powder consolidation. Among these techniques, Equal Channel Angular Pressing (ECAP)[1-4] and High Pressure Torsion (HPT)[5] are the most relevant for powder consolidation.

According to Xia[6], particles consolidation by SPD has the advantage that the surface oxide layer of particles is shattered during plastic deformation, leading to the exposal of and direct contact between metal–metal surfaces. The SPD would also be responsible for filling gaps between particles, *i.e.*, diminishing drastically the amount of porosities almost instantly. When compared to conventional PM, the densification obtained by SPD consolidation would be higher and would be achieved promptly, whereas conventional PM would need several minutes of sintering and higher energy expenditure[6].

ECAP consolidation of particles have been widely discussed in literature for many different materials, as aluminum[7,8], copper[9], titanium[10,11], metal matrix composites[12-14], pre-alloyed powders[15-17], and more recently, a mixture of dissimilar metallic powders are being studied[18,19]. The ECAP consolidation of dissimilar elemental powders can be considered a process for obtaining Deformation Processed Metal-Metal Composites (DMMCs)[20].

DMMCs can be considered a subdivision of hybrid materials[21-25] that were firstly designed for achieving great mechanical and electrical properties. Both matrix and dispersed phase are ductile metals that were heavily deformed by swaging, drawing, extrusion or rolling, which reduces the size of the phases, as well as the billet being processed[20]. Tailoring the microstructure of a composite by controlling the shape, size, distribution, and amount of the dispersed phase is crucial for achieving the desired properties[26].

*e-mail: ricardonamur@hotmail.com

Obtaining DMCCs by ECAP comes up as a great advantage, as extremely high strains can be applied without any substantial changes in the overall dimensions of the samples. Also, SPD by ECAP may produce ultrafine-grained (UFG) materials[27,28].

Studies regarding the cryogenic (~77 K) deformation of FCC metals have been developed to understand the microstructural evolution and its mechanisms[29-34]. The cryogenic deformation of metals rose as an effective route for partial suppression of dynamic recovery, thus, increasing the density of crystallographic defects. Furthermore, simultaneous improvement of strength and ductility was observed by cryogenic deformation. In this context, the cryogenic deformation of metals appears as a promising method for obtaining of DMMCs with an extremely refined microstructure.

Thus, this work focus on the obtaining of DMMCs by ECAP of blended elemental powders of commercially pure (cp) aluminum and copper at room (RT) and cryogenic temperatures (CT - ~77 K).

2. Experimental

Elemental powders of aluminum (Alcoa® - Al 99.2%, Si 0.4%, K 0.2%, Fe 0.2%) and copper (GA® - Cu 99.63%, Ca 0.23%, S 0.14%) were blended (without grinding) in a 1:1 volume ratio. This ratio was chosen to maximize the number of interfaces of the material after consolidation, thus, maximizing the areas of interest for analysis. Aluminum and Copper were chosen due to their high ductility, favoring the deformation process. Such powders were analyzed by scanning electron microscopy (SEM) for the shape and size characterization. Size characterization was performed by measuring the maximum Feret's diameter of 200 particles. The maximum Feret's diameter is defined as the longest dimension from edge to edge of a particle.

Consolidation was performed in an ECAP die with a channel angle of 90° and with a constant back pressure of 75 MPa. Pressing was performed by a manually operated hydraulic press and back pressure was applied by a previously calibrated pneumatic cylinder. Samples were obtained by a single pass at RT and at CT. The deformation at CT was performed with the submersion of the die in liquid nitrogen on an adapted styrofoam box. A picture of the system is displayed in Figure 1. Samples were also obtained with 4 passes by route Bc, *i.e.*, rotated 90° in the same direction after each pass, at RT. The estimated equivalent strain (ε) per ECAP pass in 90° dies is about 1, and minor changes are associated to the curvature angle (ψ) of the die[3].

For comparison purposes, a reference sample (cylindrical tablet with 8 mm diameter) was obtained by conventional uniaxial pressing, with a maximum pressure of 1.5 GPa, at RT

After consolidation, samples were slowly cut along its longitudinal section by a water-cooled cut off machine to avoid substantial heating, which could bring misleading information on subsequent analysis. The obtained surfaces were prepared for metallography with sandpaper (600, 800, 1200, 1500, 2000, 2500 grit) and mechanically polished with diamond paste (1 µm, 0,3 µm). Samples were not hot mounted to avoid substantial heating.

The polished surfaces were analyzed by optical microscopy (OM), which allowed the performing of automated image analysis, according to the ASTM E1245-03 standard[35], for the volumetric fraction of porosities measurement.

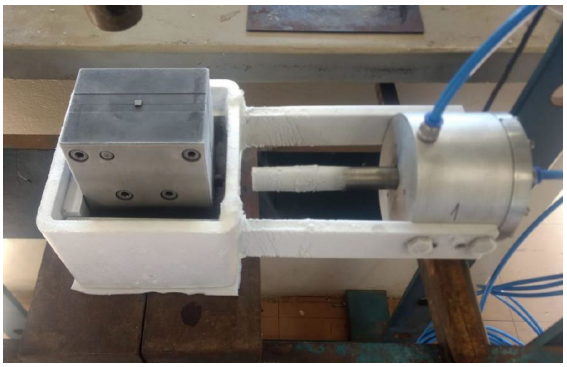

Figure 1. Picture of the ECAP system used for CT pressing.

For mechanical behavior characterization, the same polished surfaces were subjected to Vickers hardness tests. Indentations were obtained on individual particles of aluminum and copper before and after ECAP. Very low loads (10 gf for Al and 15 gf for Cu) were used to ensure that single particles were analyzed. Bulk measurements (500 gf) were also performed to analyze the composite itself. Twenty-five indentations were performed on each analysis, with 12 seconds each.

For a better understanding of the mechanical behavior of aluminum and copper under cryogenic deformation, tensile tests were performed at RT and CT, on annealed samples of commercially pure aluminum and copper. A strain rate of 1.2×10^{-3} s^{-1} was used. CT tests were performed in an apparatus developed for the immersion of the sample underneath liquid nitrogen during the whole test. The tests were performed after temperature stabilization.

A SEM coupled with energy-dispersive X-ray spectroscopy (EDX) was used for the interface analysis of the consolidated samples. Compositional maps and line scans were obtained for all samples for the identification of possible interdiffusion along the dissimilar interfaces.

Chemical etching of the samples for grain boundary analysis has proven to be quite difficult, due to the dissimilarity of the particles. Thus, X-ray diffraction (XRD) was performed as a support technique for understanding the microstructural evolution of the different metals during ECAP. As well, XRD diffraction was used for the detection of intermetallics due to interdiffusion along dissimilar interfaces. Diffraction profiles were obtained in a conventional Cu target ($K\alpha$ = 1.5406 Å) diffractometer.

2.1. Initial powder characterization

SEM images of the initial powders of aluminum and copper are displayed in Figure 2A and B, respectively. Aluminum and Copper powders presented particles with similar sizes. Aluminum particles presented a rounded shape, with some moderately elongated particles and aggregates, with a measured maximum Feret's diameter of 27.4 ± 4.8 µm. Copper particles, on the other hand, presented a mixture of spherical particles and larger irregular aggregates. Copper particles presented a maximum Feret's diameter of 25.6 ± 5.2 µm.

The average grain size measured from electron backscattered diffraction mappings (not shown here) was 3.2 ± 0.4 μm and 1.8 ± 0.4 μm for aluminum and copper, respectively.

3. Results and Discussion

3.1. Microstructure characterization

The consolidation of blended Al-Cu powders was successfully performed at RT with 1 and 4 passes, as well as 1 pass at CT. The microstructure of the longitudinal sections of these samples can be observed in Figure 3A, B and C, respectively. The microstructure of the reference sample (uniaxially pressed) can be observed in (D).

In all samples, it can be observed that aluminum and copper behave differently, where aluminum formed a continuous matrix (blue matrix) and cooper particles (orange) formed isles. In Figure 3A and C, the shape of copper particles was extremely elongated due to the shear strain imposed by ECAP.

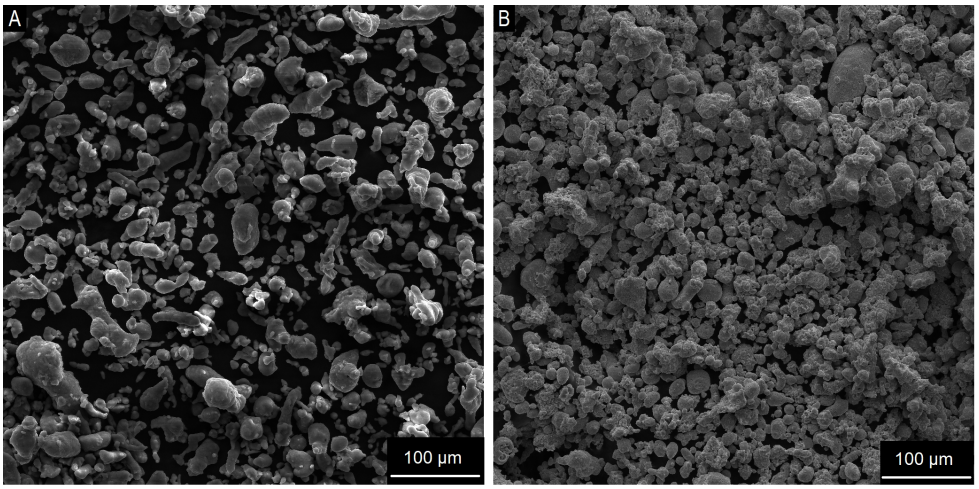

Figure 2. SEM images of the aluminum (A) and copper (B) powders.

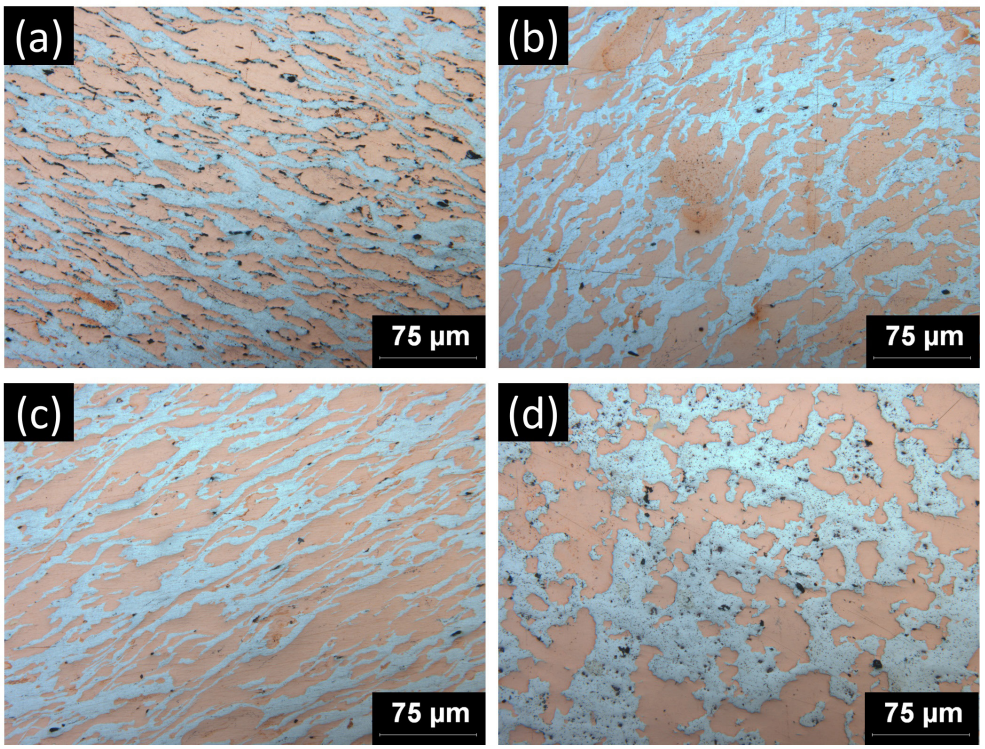

Figure 3. Optical microscopy micrographs for the samples obtained with 1 pass at RT (A), 4 passes at RT (B), 1 pass at CT (C) and by uniaxial pressing (D).

Although the accumulated strain was higher after 4 passes, it can be observed that the elongated shape of particles is less pronounced than after 1 pass. This behavior can be associated to the use of Bc route, since it is expected the restoration of the distortion on an element after 4 passes by this route[36]. Moreover, some resemblance can be noticed between Figure 3B and D, once again indicating that the restoration of the distortion was achieved to some degree.

Automated image analysis was performed for volumetric porosity quantification and results are displayed in Table 1. The values obtained indicate that ECAP is an effective method for obtaining instantaneous highly dense bulk solids, however, some considerations need to be included for a better understanding of the mechanisms involved.

Initially, it can be observed that additional passes at RT led to higher densification. It is possible that the use of multiple ECAP passes led to an efficient closure of the remnant pores of the first consolidation process. As well described by Lapovok[37,38], the ECAP shear strain along a high hydrostatic pressure (obtained using backpressure) lead to the elliptization of the defects and its closure. The structural homogeneity observed in Figure 3 indicates that 75 MPa of backpressure was sufficient for achieving such hydrostatic pressure.

When the sample consolidated with 1 pass at RT is compared to the uniaxially pressed reference sample, in Figure 3A and D, respectively, the second one achieved higher densification. Such difference can be explained by the processing pressure of both samples. The ECAPed sample was subjected to a maximum pressure of 400 MPa while was pressed through the channels, while the reference sample was uniaxially pressed until 1,5 GPa, which is much higher. An improvement of the densification of the ECAPed sample could be achieved with higher back pressure, however, it would demand a much more robust system.

On the other hand, when the densification obtained by 1 pass at RT and CT are compared, a difference of about one order of magnitude is observed. In the sample of 1 pass at CT, only a few small porosities were observed, which indicates that the shear deformation at this temperature was more efficient for consolidation and pore closure. Such behavior will be further discussed in this paper.

3.2. Mechanical behavior of pure metals at different temperatures – Tensile tests

For comparison purposes and for a better understanding of the deformation behavior at CT, tensile tests were performed in commercially pure aluminum and copper samples. The engineering strain-stress curves are displayed in Figure 4 and the true stress-strain and the work hardening rate (first derivative of the true stress) are shown in Figure 5.

Table 1. Calculated volumetric fraction of porosities for different samples.

	Volumetric fraction of porosities (%)
1 pass RT	2.86 ± 0.46
4 passes RT	0.40 ± 0.12
1 pass CT	0.37 ± 0.08
Uniaxial Pressing	1.89 ± 0.31

Also, the main results are summarized in Table 2. Each metal is further discussed in sequence.

Cp aluminum tensile tests results indicate a great increase in yield (100%) and tensile strength (88%), as well as elongation for cryogenic condition (96%). At CT, yield strength rose, due to the partial restriction to conventional plastic deformation mechanisms of aluminum at low temperatures[39]. After yield point, aluminum underwent plastic deformation with a fast-decreasing strain hardening rate, especially at RT. Aluminum is an example of a high-Stacking Fault Energy (SFE) fcc metal (SFE ≅ 165 $mJ.m^{-2}$ at RT), facilitating the cross slip of screw dislocations and dynamic recovery, especially at higher homologous temperatures (T_h = 0.32 at RT)[40]. The less abrupt decrease in the strain hardening rate at CT indicates that dynamic recovery was partially inhibited due to the lower homologous temperature (T_h = 0.08 at 77 K).

Copper, analogously to aluminum, presented great increases in tensile strength (59.7%) and elongation (96%) for CT tests. The ductility improvement in CT may be associated with the large storage of defects and strain energy simultaneously with dynamic recovery inhibition at such low homologous temperature (T_h = 0.06 at 77 K, while T_h = 0.22 at RT)[41,42]. In addition, cryodeformation of copper induces mechanical twinning, besides dislocation glide, as observed in previous works, due to its low SFE (SFE ≅ 70 $mJ.m^{-2}$ at RT)[40,42]. The occurrence of twinning and dislocation movement in CT is, possibly, the main reason for the high work hardening rate obtained and the ductility increase in this material, as seen in Figure 5[42,43]. Once again, a higher work hardening rate was obtained at CT (Figure 5), indicating that dynamic recovery was efficiently inhibited and more microstructural defects were stored. Compared to cp aluminum, cp copper presents a higher strain hardening rate, thus, it can be strain hardened more efficiently according to the lower SFE.

Especially for copper, slip and twinning are considered competitive deformation mechanisms, and constitutive approaches were developed to predict the critical stress for twinning, as a function of external (temperature, strain rate) and internal (grain size, SFE) parameters[44]. It is known that lowering the SFE and deformation temperatures promotes

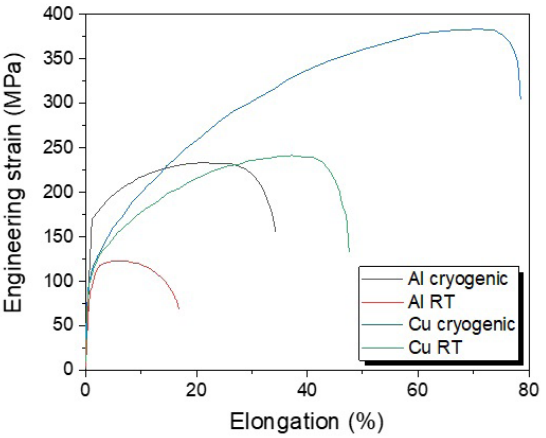

Figure 4. Stress-strain behavior at RT and CT for cp aluminum and cp copper.

Table 2. Comparison between tensile tests at RT and CT for aluminum and copper.

	Cp Aluminum (RT)	Cp Aluminum (CT)	Cp copper (RT)	Cp copper (CT)
Yield strength (MPa)	85	170	105	105
Ultimate tensile strength (MPa)	123.5	233	240.7	384.5
Elongation to failure (%)	17.6	34.5	47.6	78.5
Yield strength increase at CT (%)	-	100	-	0
Ultimate tensile strength increase at CT (%)	-	88	-	59.7
Elongation increase at CT (%)	-	96	-	64.9
Uniform elongation (%)	5.1	24.2	38.6	71.7
True strain at the onset of plastic instability (Considerè criterion)	0.06	0.2	0.31	0.53

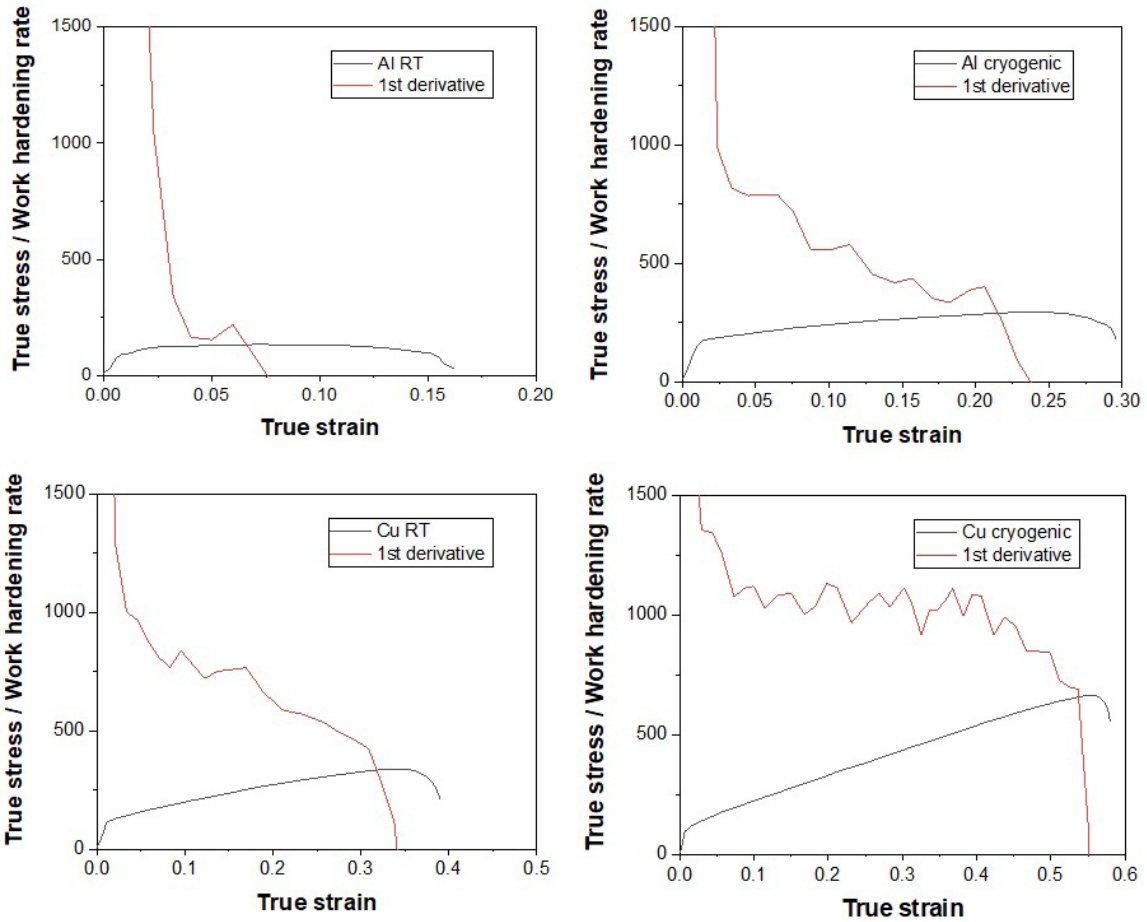

Figure 5. Engineering Stress-strain behavior at RT and CT for cp aluminum and cp copper (left column) and True stress and work hardening rate as a function of true strain (Considerè criterion) (right column).

twinning over dislocation slip, and slip is highly sensitive to external parameters, while twinning is much less sensitive to these parameters[45]. According to the constitutive model of Meyers et al.[44], the critical stress for twinning in a 10 µm grain-sized copper is roughly 500 MPa at a large range of temperatures encompassing the ones used in the present work. From Figure 5, one can observe that the true stress surpassed such value for the cp copper tested at CT, but it did not surpass it in the test carried out at RT. Based on this fact, is reasonable to assume that twinning plays a major role in the deformation of the cp copper at CT but not at RT.

Deformation twins can be a pragmatic approach to reach significant grain refinement and homogeneous microstructures and, consequently, improved plastic strain behavior[46].

SEM images of the fracture surfaces for both metals and both temperatures were obtained, as displayed in Figure 6.

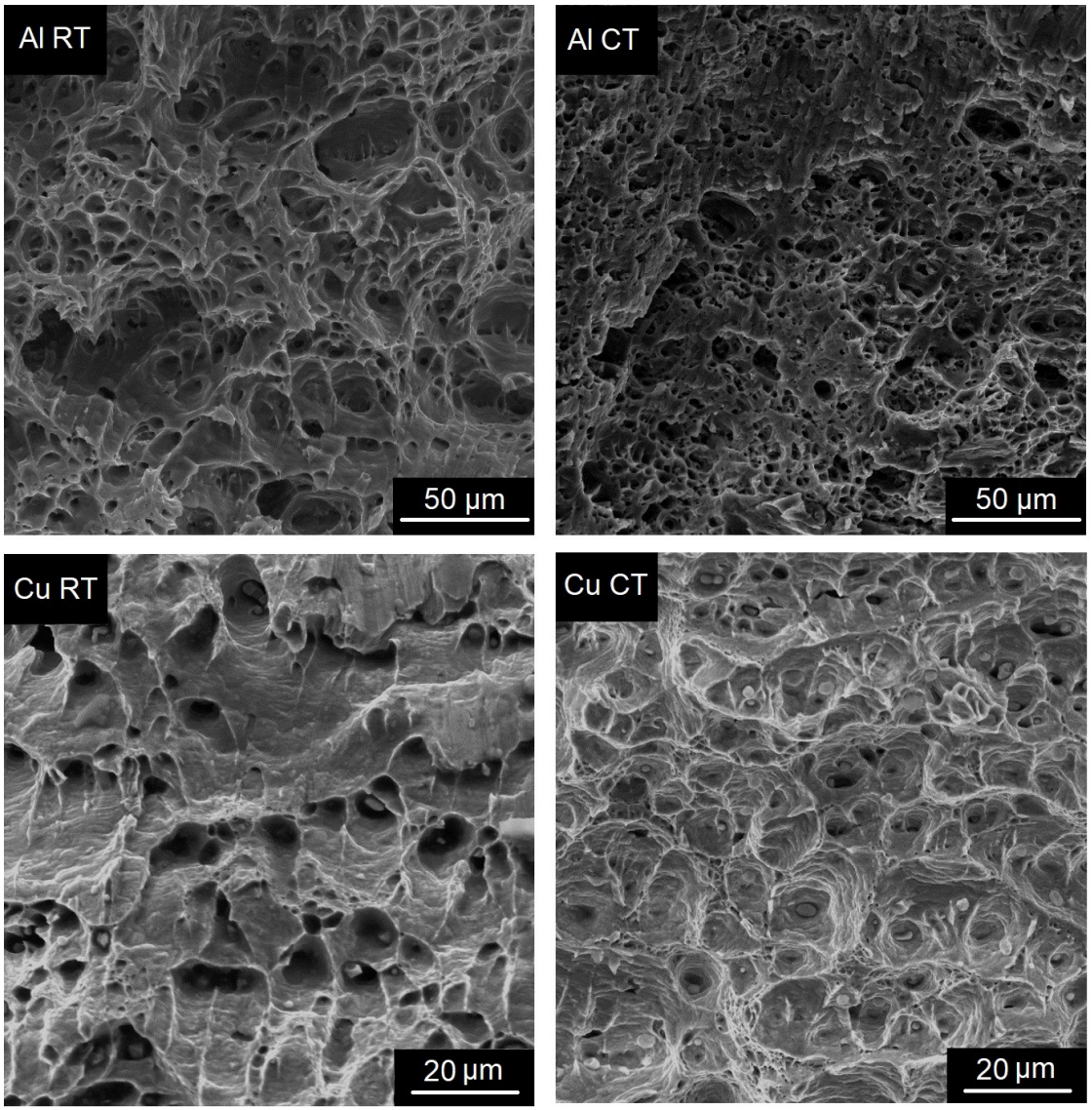

Figure 6. SEM fractographies for cp Al and cp Cu samples tested at RT and CT.

Both at RT and CT, fracture surfaces are mainly composed of dimples. At CT, the fracture surface dimples are smaller for both metals.

The ductility and uniform elongation improvement at CT may be explained by the achievement of a stable deformation state of the sample prior to fracture as described by Glazer et al.[47], and Gregson and Flower[48]. To quantify it, a mathematical approach can be used for defining the onset of the plastic instability on metals, which is the Considerè criterion[49]. This criterion was calculated using the true stress-strain curves of the tensile tests (Figure 5), and the values displayed in Table 2 represent the true strain at the onset of plastic instability.

The results for the Considerè criterion indicate that plastic instability begins at low true strains of 0.06 for the cp aluminum tested at RT. On the other hand, at CT, plastic instability started at a true strain of 0.2. This increase is caused by the higher strain hardening rate, since work hardening tends to stabilize the plastic deformation and increase the uniform elongation. The same tendency was observed for copper, where the calculated Considerè criterion was 0.31 at RT and 0.53 at CT. Finally, the tensile tests have proven useful for a better understanding of the substantial improvement on the densification of blended elemental powders of Al-Cu.

3.3. Mechanical behavior of the DMMC - Hardness tests

Vickers hardness was performed in the initial powders and in the ECAPed samples. Results are displayed in Table 3.

At RT, aluminum particles presented a Vickers hardness (HV) increase of 50.1% after the first ECAP pass and 61.1% after four passes. This behavior corroborates the results obtained during the tensile tests for cp aluminum, where its high SFE and moderately high homologous temperature may have led to poor strain hardenability. Nevertheless, the particles consolidated at CT presented a hardness increase

Table 3. Vickers hardness (HV) for initial powders and for the respective elements after ECAP passes at RT and CT. Bulk measurements of the composite is also displayed.

	Aluminum (HV)	Copper (HV)
Initial powder	49.9 ± 2.9	71.33 ± 3.3
Uniaxial pressing	54.3 ± 2.2	139.7± 7.2
	(↑ 8.8%)	(↑ 95.9%)
1 pass RT	74.9 ± 3.9	163.3 ± 12.6
	(↑ 50.1%)	(↑ 129%)
4 passes RT	80.4 ± 3.7	181 ± 5.6
	(↑ 61.1%)	(↑ 153.7%)
1 pass CT	80.9 ± 2.9	186.1 ± 6.6
	(↑ 62.1%)	(↑ 160.9%)
	Bulk measurements (HV)	
Al-Cu 1 pass RT	90.6 ± 3.2	
Al-Cu 4 passes RT	104 ± 2.5	
Al-Cu 1 pass CT	102.1 ± 3.1	
Uniaxial pressing	72.3 ± 7.1	

of 62.1% after 1 pass, which is higher than 4 passes at RT. This result indicates that the CT pressing of aluminum was effective in partially inhibiting the dynamic recovery and leading to a harder structure. At the same time, the harder structure obtained at CT was also more ductile, which allowed a more efficient pore closure during ECAP.

At RT, copper, similarly, presented a higher hardness increase during the first pass (129%), however, it was much higher than aluminum. After 4 passes, the hardness increased 153.7%, indicating a higher strain hardenability when compared to aluminum. As well as aluminum, the copper particles pressed at CT presented a hardness increase similar to 4 passes at RT, with the advantage of producing a much more ductile and uniform deformation.

An unusual behavior was observed for the uniaxially pressed powders, where aluminum hardness was increased by 8.8%, whereas copper hardness was increased by 95.9%. Such difference was probably motivated by the difference between the elastic modulus of copper (128 GPa) and aluminum (62 GPa), creating a stress shielding phenomenon[50]. Using simulations, Martin and Bouvard have already demonstrated that the uniaxial compression of blended powders with a great difference of hardness may lead to a retardation of the deformation of the softer particles. Simulation results indicate that a network of hard particles is capable of bearing most of the applied load, obstructing the deformation of the softer particles[51].

Bulk measurements indicate that the hardness of the composite itself is lower than the average hardness between aluminum and copper particles. Many factors may have influenced this result, as the detachment of aluminum/copper interfaces and remnant pores. Thus, in this experimental condition, the rule of mixtures for the hardness of composites was not satisfied.

3.4. SEM/EDX analysis

The compositional maps obtained are shown in Figure 7 and line scans are displayed in Figure 8.

The analysis of compositional maps and line scans indicates that interdiffusion does not happened extensively along the interfaces.

Although SPD processed powders are prone to an improved diffusivity, due to the shattering of the superficial oxide of the particles[6] and the amorphization of such oxides when they are not completely withdraw[52], it was not observed in these experimental conditions. In recent works by Namur et al.[18,19], the same behavior was observed for blended powders of Fe-Cr-Ni / Fe-Mn-Al and substantial mass transfer was only obtained by the heat treatment of the samples, which led to a much more complex microstructure.

As a comparison, Castro and collaborators[53] used room temperature HPT to consolidate metallic particles of Mg and Zn. The authors produced nanostructured metal-matrix composites with a wide range of compositions (from 20 wt% to 95% Zn) using 3.8 GPa, 10 and 20 HPT turns at 1 rpm. One of the findings of the authors is that mechanical deformation is fundamental for mixing the phases and diffusion contributes to the formation of intermetallics, especially $MgZn_2$ at Zn segregations along Mg grain boundaries. It should be highlighted that the equivalent strain in Castro's experiment is considerably higher than what was applied by ECAP in this work.

3.5. X-ray diffraction

Figure 9A displays the diffractograms obtained for the initial powders and Figure 9B shows the diffractograms for all the ECAPed samples. By comparing Figure 9A and B, it can be observed that all peaks associated with the source powders remained and additional peaks were not detected. This result corroborates with the SEM-EDX analysis, where interdiffusion was not substantially observed, thus, not leading to any phase transformation.

The same diffratograms were analyzed by using the PANalitycal High Score Plus software. Figure 10A and B shows the variation of average microstrain, compared to hardness variation, of the initial powders and after ECAP for aluminum and copper, respectively. The microstrain <ε> calculation was performed based on the Stokes-Wilson approximation[54]:

$$\langle \varepsilon \rangle = \frac{\beta^{(hkl)}}{4\tan(\theta)}$$

Where β is the FWHM (full width at half maximum) of the sample for a given peak and θ is the Bragg angle. Instrumental contribution for peak broadening was removed by previous fit of a CeO_2 standard and by considering Gaussian-shaped peaks.

The analysis of Figure 10 indicates a close agreement between the hardness and the lattice average microstrain, especially for 1 and 4 passes at RT. On the other hand, the variation of the average microstrain after 1 pass at CT is similar to the average microstrain after 1 pass at RT, and the same trend was not observed for the hardness, whose variation was more substantial.

This result may indicate that the sum of the deformation mechanisms that are active at CT, helps the increase on hardness, nevertheless, are similar on what concerns the average microstrain of the lattice. This hypothesis is especially reasonable for copper, with a lower SFE than aluminum and known as a metal prone for mechanical twinning at low temperatures[31,43,55].

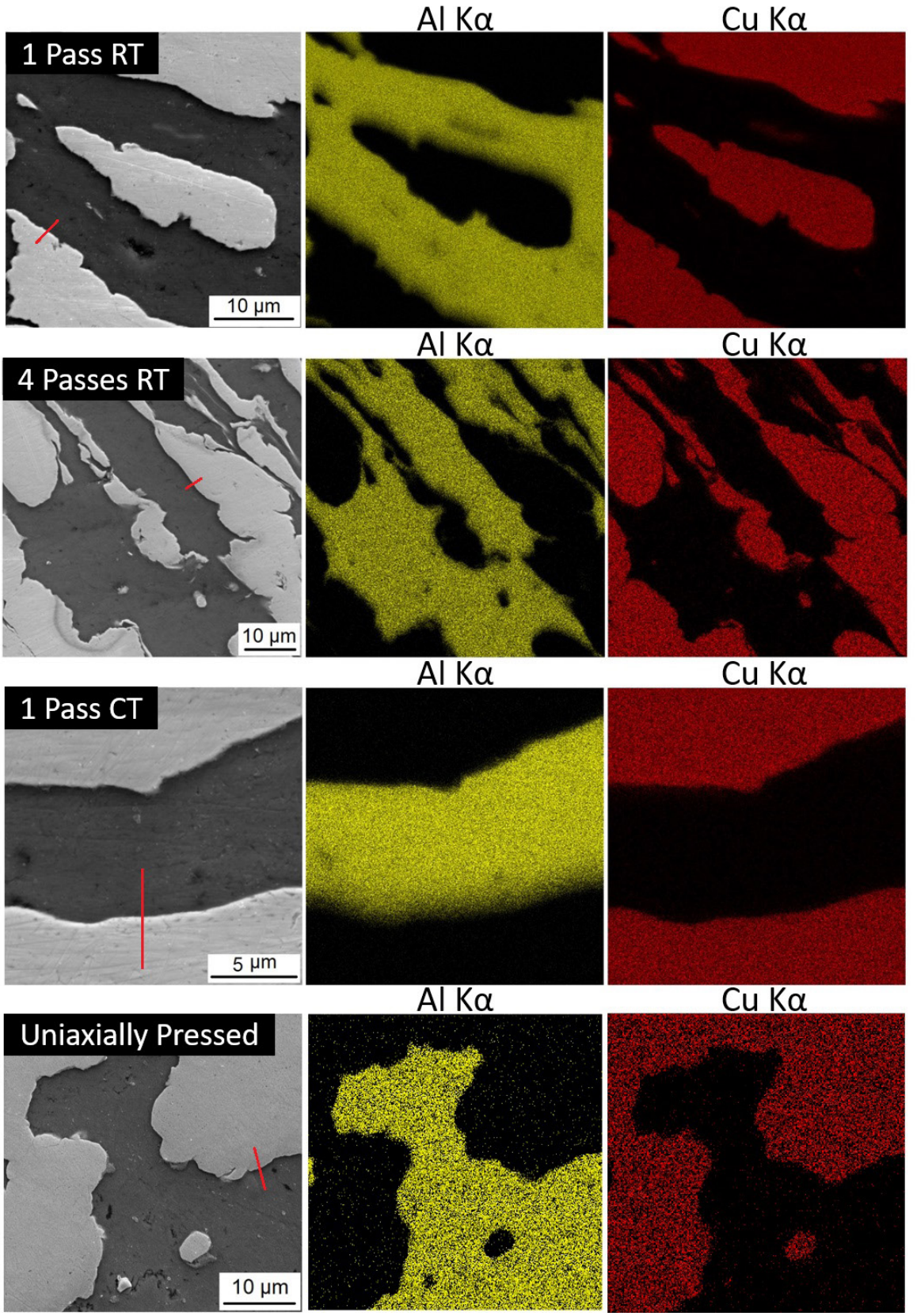

Figure 7. SEM-EDX analyzed area and compositional maps on different samples. The red lines in the first column represents where line scans were obtained.

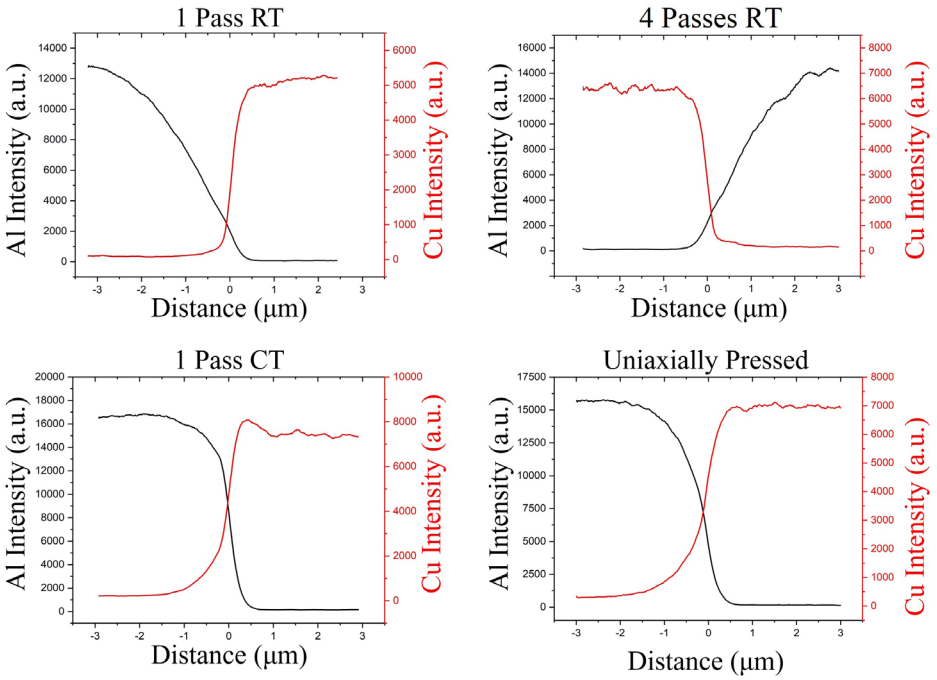

Figure 8. SEM-EDX line scans for the interface between Al and Cu particles on different samples. The location of the line scans is displayed by red lines in the first column of Figure 7.

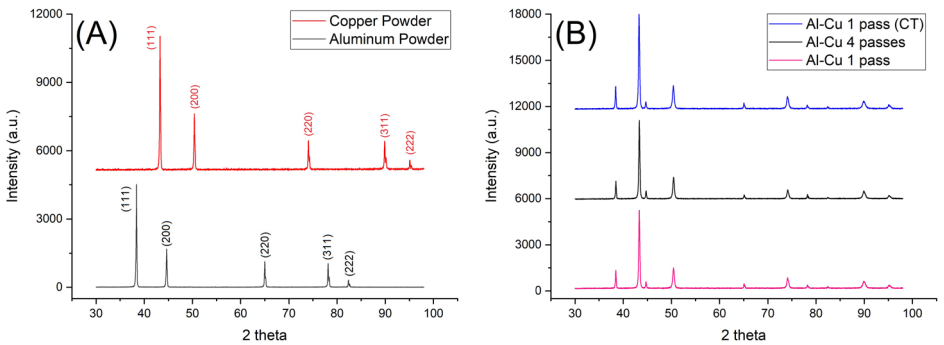

Figure 9. XRD diffractogram for the initial powders of aluminum and copper (A) and for the samples after ECAP (B).

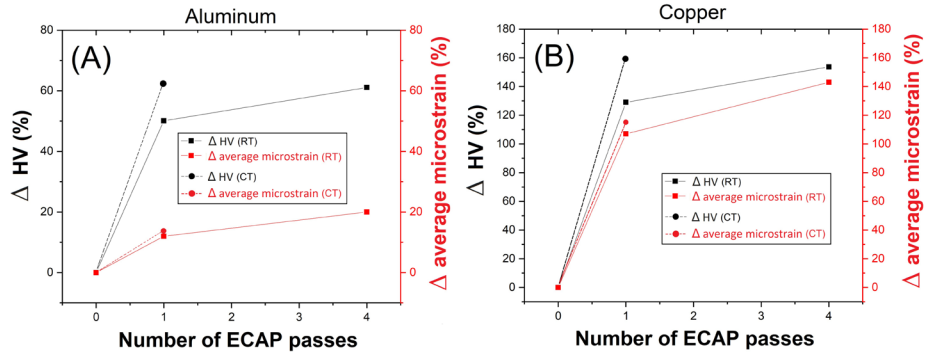

Figure 10. Variation of hardness and microstrain for aluminum (A) and copper (B) on different samples.

4. Conclusions

Blended elemental powder of aluminum and copper were successfully consolidated at room and at cryogenic temperatures. Based on the experimental evidences presented, the following conclusions may be drawn:

1. The consolidation of Al – Cu powders have proven to be more efficient at cryogenic temperature, with densification higher than 99.5%. Room temperature consolidation produced more porous samples.
2. Additional ECAP passes at room temperature led to an improvement in the densification of the samples, as well as a recovery of the structural distortion after 4 passes by the route Bc.
3. After ECAP, the hardness (HV) of the metals was substantially increased, especially copper. The higher hardness increase was obtained during the first ECAP pass for both metals. The hardness obtained after 1 pass of cryogenic ECAP was even higher than after 4 ECAP passes at room temperature.
4. Tensile tests of cp Aluminum and Copper indicated that a simultaneous increase in strength and ductility can be achieved at cryogenic temperature. This result corroborates the findings on the hardness tests and on the densification measurements.
5. SEM-EDX and XRD were performed, but extensive interdiffusion was not observed, as well as phase transformations.
6. XRD measurements indicated a trend on the increase of average microstrain with ECAP passes. A similar trend was observed with the variation of hardness, with a possible correlation.

5. Acknowledgements

The authors acknowledge C-Labmu for the use of its infrastructure. The authors RSN and MSA acknowledge CAPES for the scholarship.

6. References

1. Segal VM, Reznikov VI, Drobyshevskii AE, Kopylov VI. Plastic working of metals by simple shear. Russ Metall. 1981;1:99-105.
2. Segal VM. Materials processing by simple shear. Mater Sci Eng A. 1995;197(2):157-64.
3. Valiev RZ, Langdon TG. Principles of equal-channel angular pressing as a processing tool for grain refinement. Prog Mater Sci. 2006;51(7):881-981.
4. Mendes Filho AA, Prados EF, Valio GT, Rubert JB, Sordi VL, Ferrante M. Severe plastic deformation by equal channel angular pressing: product quality and operational details. Mater Res. 2011;14(3):335-9.
5. Edalati K, Horita Z. A review on high-pressure torsion (HPT) from 1935 to 1988. Mater Sci Eng A. 2016;652:325-52.
6. Xia K. Consolidation of particles by severe plastic deformation: mechanism and applications in processing bulk ultrafine and nanostructured alloys and composites. Adv Eng Mater. 2010;12(8):724-9.
7. Senkov ON, Senkova SV, Scott JM, Miracle DB. Compaction of amorphous aluminum alloy powder by direct extrusion and equal channel angular extrusion. Mater Sci Eng A. 2005;393(1-2):12-21.
8. Xia K, Wu X. Back pressure equal channel angular consolidation of pure Al particles. Scr Mater. 2005;53(11):1225-9.
9. Haouaoui M, Karaman I, Harwig KT, Maier HJ. Microstructure evolution and mechanical behavior of bulk copper obtained by consolidation of micro- and nanopowders using equal-channel angular extrusion. Metall Mater Trans, A Phys Metall Mater Sci. 2004;35(9):2935-49.
10. Luo P, Xie H, Paladugu M, Palanisamy S, Dargusch MS, Xia K. Recycling of titanium machining chips by severe plastic deformation consolidation. J Mater Sci. 2010;45(17):4606-12.
11. Luo P, Mcdonald DT, Xu W, Palanisamy S, Dargusch MS, Xia K. A modified Hall-Petch relationship in ultrafine-grained titanium recycled from chips by equal channel angular pressing. Scr Mater. 2012;66(10):785-8.
12. Parasiris A, Hartwig KT. Consolidation of advanced WC-Co powders. Int J Refract Met Hard Mater. 2000;18(1):23-31.
13. Poletti C, Balog M, Schubert T, Liedtke V, Edtmaier C. Production of titanium matrix composites reinforced with SiC particles. Compos Sci Technol. 2008;68(9):2171-7.
14. Haghighi RD, Jahromi SAJ, Moresedgh A, Khorshid MT. A comparison between ECAP and conventional extrusion for consolidation of aluminum metal matrix composite. J Mater Eng Perform. 2012;21(9):1885-92.
15. Lapovok R, Tomus D, Muddle BC. Low-temperature compaction of Ti-6Al-4V powder using equal channel angular extrusion with back pressure. Mater Sci Eng A. 2008;490(1-2):171-80.
16. Bera S, Chowdhury SG, Estrin Y, Manna I. Mechanical properties of Al7075 alloy with nano-ceramic oxide dispersion synthesized by mechanical milling and consolidated by equal channel angular pressing. J Alloys Compd. 2013;548:257-65.
17. Lapovok R, Tomus D, Bettles B. Shear deformation with imposed hydrostatic pressure for enhanced compaction of powder. Scr Mater. 2008;58(10):898-901.
18. Namur RS, Feitosa LM, Ferreira ACK, Bueno AG, Zilnyk KD, Cintho OM. Ecap consolidation and heat treatment of blended elemental powders of Iron, Chromium, Nickel and Manganese. Mater Res. 2019;22(Suppl. 1):e20180869.
19. Namur RS, Ferreira ACK, Feitosa LM, Bueno AG, Zilnyk KD, Cintho OM. Equal channel angular pressing consolidation and heat treatment of blended elemental powders of Fe-Mn-Al. Mater Sci Forum. 2020;1012:291-5.
20. Russell AM, Chumbley LS, Tian Y. Deformation-processed metal/metal composites. Adv Eng Mater. 1991;1:11-22.
21. Khoddam S, Tian L, Sapanathan T, Hodgson PD, Zarei-Hanzaki A. Latest developments in modeling and characterization of joining metal based hybrid materials. Adv Eng Mater. 2018;20(9):1800048.
22. Medvedev AE, Lapovok R, Koch E, Höppel HW, Göken M. Optimisation of interface formation by shear inclination: example of aluminium-cooper hybrid produced by ECAP with back-pressure. Mater Des. 2018;146:142-51.
23. Kocich R, Kunčická L, Macháčková A, Šofer M. Improvement of mechanical and electrical properties of rotary swaged Al-Cu clad composites. Mater Des. 2017;123:137-46.
24. Russell AM, Lund T, Chumbley LS, Laabs FA, Keehner LL, Harringa JL. A high-strength, high-conductivity Al-Ti deformation processed metal metal matrix composite. Compos, Part A Appl Sci Manuf. 1999;30(3):239-47.
25. Xu K, Russell AM, Chumbley LS, Laabs FC, Gantovnik VB, Tian Y. Characterization of strength and microstructure in deformation processed Al-Mg composites. J Mater Sci. 1999;34(24):5955-9.
26. Meyers MA, Chawla KK. Mechanical behavior of materials. Cambridge: Cambridge University Press; 2008.
27. Valiev RZ, Islamgaliev RK, Alexandrov IV. Bulk nanostructured materials from severe plastic deformation. Prog Mater Sci. 2000;45(2):103-89.
28. Valiev RZ, Korznikov AV, Mulyukov RR. Structure and properties of ultrafine-grained materials produced by severe plastic deformation. Mater Sci Eng A. 1993;168(2):141-8.

29. Magalhães DCC, Hupalo MF, Cintho OM. Natural aging behavior of AA7050 Al alloy after cryogenic rolling. Mater Sci Eng A. 2014;593:1-7.
30. Maeda MY, Quintero JJH, Izumi MT, Hupalo MF, Cintho OM. Study of cryogenic rolling of FCC metals with different stacking fault energies. Mater Res. 2017;20(Suppl. 2):716-21.
31. Edalati K, Cubero-Sesin JM, Alhamidi A, Mohamed IF, Horita Z. Influence of severe plastic deformation at cryogenic temperature on grain refinement and softening of pure metals: investigation using high-pressure torsion. Mater Sci Eng A. 2014;613:103-10.
32. Crivoi MR, Hoyos JJ, Izumi MT, Aguiar DJM, Namur RS, Terasawa AL, et al. In situ analysis of cryogenic strain of AISI 316L stainless steel using synchrotron radiation. Cryogenics. 2020;105:103020.
33. Izumi MT, Quintero JJH, Crivoi MR, Maeda MY, Namur RS, Aguiar DJM, et al. In situ X-ray diffraction analysis of face-centered cubic metals deformed at room and cryogenic temperatures. J Mater Eng Perform. 2019;28(8):4658-66.
34. Namur RS, Huber DE, Ramirez AJ, Cintho OM. In situ analysis of cryoformed metals by STEM. Microsc Microanal. 2019;25(S2):916-7.
35. ASTM: American Society for Testing and Materials. ASTM E1245-03. West Conshohocken: ASTM International; 2016.
36. Furukawa M, Iwahashi Y, Horita Z, Nemoto M, Langdon TG. The shearing characteristics associated with equal-channel angular pressing. Mater Sci Eng A. 1998;257(2):328-32.
37. Lapovok R. The role of back-pressure in equal channel angular extrusion. J Mater Sci. 2005;40(2):341-6.
38. Lapovok R. Damage evolution under severe plastic deformation. Int J Fract. 2002;115:159-72.
39. Kula EB, DeSisto TS. Plastic behavior of metals at cryogenic temperatures. In: Schwartzberg F, editor. Behavior of materials at cryogenic temperatures. West Conshohocken: ASTM International; 2009.
40. Cabibbo M, Santecchia E. Early stages of plastic deformation in Low and High SFE Pure Metals. Metals (Basel). 2020;10(6):751-66.
41. Wang Y, Chen M, Zhou F, Ma E. High tensile ductility in a nanostructured metal. Nature. 2002;419(6910):912-5.
42. Zhao YH, Bingert JF, Liao XZ, Cui BZ, Han K, Sergueeva AV, et al. Simultaneously increasing the ductility and strength of ultra-fine-grained pure copper. Adv Mater. 2006;18(22):2949-53.
43. Konkova T, Mironov S, Korznikov A, Semiatin SL. Microstructure instability in cryogenically deformed copper. Scr Mater. 2010;63(9):921-4.
44. Meyers MA, Vöhringer O, Lubarda VA. The onset of twinning in metals: a constitutive description. Acta Mater. 2001;49(19):4025-39.
45. Sarma VS, Wang J, Jian WW, Kauffmann A, Conrad H, Freudenberger J, et al. Role of stacking fault energy in strengthening due to cryo-deformation of FCC metals. Mater Sci Eng A. 2010;527(29-30):7624-30.
46. Gong YL, Wen CE, Wu XX, Ren SY, Cheng LP, Zhu XK. The influence of strain rate, deformation temperature and stacking fault energy on the mechanical properties of Cu alloys. Mater Sci Eng A. 2013;583:199-204.
47. Glazer J, Verzasconi SL, Sawtell RR, Morris JW. Mechanical behavior of aluminum-lithium alloys at cryogenic temperatures. Metall Trans, A, Phys Metall Mater Sci. 1987;18(10):1695-701.
48. Gregson PJ, Flower HM. Microstructural control of toughness in aluminium-lithium alloys. Acta Metall. 1985;33(3):527-37.
49. Yasnikov IS, Vinogradov A, Estrin Y. Revisiting the Considère criterion from the viewpoint of dislocation theory fundamentals. Scr Mater. 2014;76:37-40.
50. Niinomi M, Hatoori T, Niwa S. Material characteristics and biocompatibility of low ridigity titanium alloys for biomedical applications. In: Yaszemski MJ, editor. Biomaterials in orthopedics. Boca Raton: CRC Press; 2004.
51. Martin CL, Bouvard D. Study of the cold compaction of composite powders by the discrete element method. Acta Mater. 2003;51(2):373-86.
52. Ng HP, Haase C, Lapovok R, Estrin Y. Improving sinterability of Ti-6Al-4V from blended elemental powders through equal channel angular pressing. Mater Sci Eng A. 2013;565:396-404.
53. Castro MM, Montoro LA, Isaac A, Kawasaki M, Figueiredo RB. Mechanical mixing of MG and Zn using high-pressure torsion. J Alloys Compd. 2021;869:159302.
54. Stokes AR, Wilson AJC. The diffraction of x rays by distorted crystal aggregates – I. Proc Phys Soc. 1944;56(3):174-81.
55. Konkova T, Mironov S, Korznikov A, Semiatin SL. Microstructural response of pure copper to cryogenic rolling. Acta Mater. 2010;58(16):5262-73.